

Multi-Source Adaptive Generative Augmentation for Quality-Driven Contrastive Representation Learning

Xiaojie Li^{1,2} Bei Wang¹ Jianlong Wu¹ Yue Yu² Liqiang Nie¹ Min Zhang¹

¹Harbin Institute of Technology, Shenzhen ²Peng Cheng Laboratory

xiaojieli0903@gmail.com, wangbei010118@gmail.com, wujianlong@hit.edu.cn

yuy@pcl.ac.cn, nieliqiang@gmail.com, zhangmin2021@hit.edu.cn

Abstract

The efficacy of contrastive learning hinges on the construction and utilization of high-quality positive pairs. However, current methods face critical limitations on two fronts: on the construction side, handcrafted and rigid generative augmentations often struggle to balance diversity with semantic fidelity due to a lack of fine-grained controllability; on the learning side, the absence of quality assessment leads to suboptimal supervision where noisy and high-quality pairs are treated equally. To tackle these challenges, we propose GenView++, a unified framework that introduces two synergistic innovations. First, to improve pair construction, we introduce a multi-source adaptive view generation mechanism. This offline module synthesizes diverse yet semantically coherent views by dynamically modulating generative parameters based on input characteristics like visual saliency and caption complexity. Second, to optimize pair utilization, we propose a quality-driven contrastive learning mechanism that assesses each pair’s semantic alignment and visual diversity. It dynamically reweights the training objective to prioritize informative pairs while suppressing redundant or misaligned ones. Extensive experiments demonstrate the effectiveness of GenView++ across both vision and vision–language tasks. For vision representation learning, it improves MoCov2 by +2.5% on ImageNet linear classification. For vision–language learning, it raises the average zero-shot classification accuracy by +12.31% over CLIP and +5.31% over SLIP across ten datasets, and further improves Flickr30k text retrieval R@5 by +3.2%. The code is available at <https://github.com/xiaojieli0903/GenViewPlusPlus>.

1. Introduction

Self-supervised learning (SSL) has emerged as a fundamental paradigm for acquiring robust and generalizable representations from large-scale unlabeled data. Among var-

ious SSL methods, contrastive learning (CL) [7, 10] has achieved remarkable success in both *vision* [25, 30, 31] and *vision-language* [46, 60] domains. The core principle of CL is to learn invariant and discriminative representations by maximizing the similarity between different views of the same instance (positive pairs) while pushing them apart from other instances. Its effectiveness hinges on a critical trade-off in constructing positive pairs: they must be *semantically consistent* to ensure true invariance, yet *sufficiently diverse* to foster robust generalization.

However, constructing such optimal pairs remains a persistent challenge. Traditional methods rely on handcrafted augmentations (e.g., cropping, color jittering), which modify only surface-level statistics. These transformations often yield redundant views with *limited diversity* (Fig. 1 a-1, a-4) or, when applied aggressively, risk *semantic corruption* by cropping out essential content (a-2, a-3). This issue is exacerbated in vision–language pretraining, where visual distortions can break the critical alignment between the image and its textual caption. Recent advances propose using generative models (e.g., Stable Diffusion [62]) to synthesize diverse views. While promising, integrating these models into CL is non-trivial due to a lack of *fine-grained controllability*. Existing generative augmentation methods [72, 85, 91] typically rely on a single conditioning modality (either image or text) and fixed generation parameters. This rigid approach fails to adapt to the complexity of individual samples, often leading to a mismatch where simple samples are over-distorted (semantic drift) or complex samples are under-varied (redundancy). Furthermore, unimodal conditioning overlooks the synergistic potential of joint image-text pairs to guide more precise synthesis.

Compounding these **construction-side** issues is a limitation on the **learning side**: the absence of *pair-level quality assessment*. Current pipelines operate on a uniform assumption, treating every positive pair, whether high-quality, redundant, or noisy, as equally important (gray scores in Fig. 1 a). This indiscriminate supervision forces models to overfit to false positives generated by aggressive augmenta-

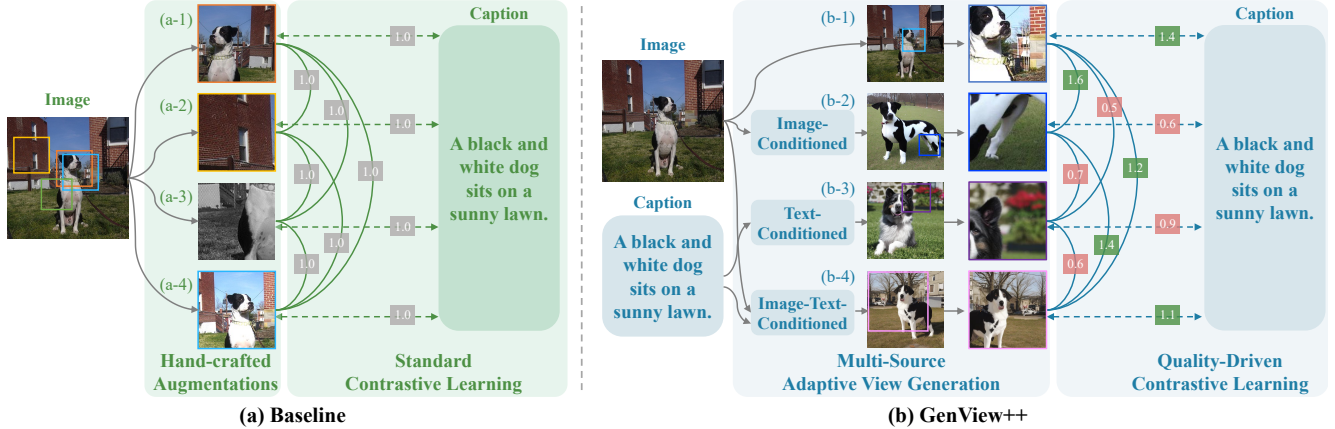


Figure 1. **Motivation.** (a) Standard contrastive learning methods rely on handcrafted augmentations, which provide limited diversity, risk semantic distortions, and lack pair-level quality control during training. (b) GenView++ addresses these limitations via (i) **Multi-Source Adaptive View Generation** synthesizes diverse and semantically aligned views, and (ii) **Quality-Driven Contrastive Learning** reweights supervision by assessing the quality of both image–image and image–text pairs.

tions or noisy web data [63, 65], ultimately degrading representation quality.

To address these challenges in vision-only pretraining, our preliminary work, **GenView** [47] (ECCV 2024), proposed a controllable framework. It introduced an *adaptive view generation* strategy that perturbs image embeddings based on foreground saliency to strictly balance diversity and fidelity. Furthermore, it designed a *quality-driven contrastive learning* mechanism to reweight image–image pairs based on their semantic overlap. While effective for visual tasks, GenView is inherently limited by its reliance on a single image modality. It overlooks the rich semantic guidance available in text, restricting its ability to construct high quality pairs for vision–language representation learning.

To overcome these limitations and generalize these principles to the multimodal domain, we propose **GenView++**, a unified framework that introduces two synergistic innovations: a multi-source adaptive view generation mechanism to construct better pairs, and an extended quality-driven supervision mechanism to utilize them effectively.

First, we introduce a **Multi-Source Adaptive View Generation** module. Unlike fixed strategies, this offline mechanism dynamically modulates the trade-off between diversity and fidelity based on the input’s characteristics. It integrates three adaptively controlled conditioning strategies. **(1) Image-Conditioned Mode** (Fig. 1 b-2): Inherited from GenView, it enhances visual invariance. We employ a saliency-aware strategy where low-saliency subjects receive weaker perturbations to preserve semantic identity, while high-saliency subjects allow stronger perturbations to enrich diversity. **(3) Text-Conditioned Mode** (Fig. 1 b-3): We leverage captions to guide synthesis, dynamically tuning guidance strength based on *caption complexity*. *Intuitively*, simple or abstract captions require stronger guidance to prevent semantic drift, whereas complex, descrip-

tive captions allow for relaxed guidance to foster creative transformations without losing context. **(3) Image-Text-Conditioned Mode** (Fig. 1 b-4): By synergistically adapting both image noise and text guidance, this mode produces views that are visually diverse, semantically consistent, and textually grounded, effectively bridging the modality gap.

Second, we introduce an extensible **Quality-Driven Contrastive Learning** mechanism. Unlike the uniform “augment-and-trust” paradigm, we explicitly evaluate and reweight each pair. For *image–image pairs*, we reward high foreground consistency and background diversity. For *image–text pairs*, we introduce a novel metric combining *cross-modal alignment* (via CLIP similarity) and *visual diversity*. This mechanism dynamically amplifies high-quality pairs (green scores in Fig. 1 b) while suppressing redundant or misaligned ones (red scores), ensuring that the generated views are utilized with maximum effectiveness.

Our contributions are as follows:

- We propose GenView++, a unified framework that extends the principles of adaptive generation and quality-driven supervision to simultaneously enhance vision and vision–language representation learning.
- We introduce a multi-source adaptive view generation module. By dynamically modulating generation parameters based on input characteristics, it balances the trade-off between semantic fidelity and diversity.
- We develop a quality-driven contrastive loss for both image–image and image–text pairs. It explicitly assesses pair quality to prioritize informative samples while mitigating the impact of noise from generation or web data.
- Extensive experiments demonstrate that GenView++ consistently outperforms strong baselines. For vision tasks, it improves MoCov2 and BYOL; for vision–language tasks, it outperforms CLIP and StableRep, raising zero-shot classification accuracy by **+12.31%** over CLIP.

2. Related Work

2.1. Contrastive Representation Learning

Self-supervised learning (SSL) has evolved from pretext tasks [24, 53, 57, 74] to two dominant paradigms: Masked Image Modeling (MIM) and Contrastive Learning (CL). While MIM approaches like MAE [31] have achieved impressive results in fine-tuning tasks by reconstructing missing pixels, CL [2, 4, 10, 12, 30, 54, 70, 80] remains superior in learning linearly separable global representations and robust zero-shot transferability. By maximizing similarity between positive pairs while pushing apart negatives, CL learns invariant representations. Non-contrastive approaches [1, 6, 7, 11, 20, 25, 45, 88] further remove the need for negative pairs using asymmetric networks. In the vision-language (VL) domain, models such as CLIP [60], ALIGN [38], and BLIP [46] extend this principle to cross-modal pairs from massive web datasets. Despite their success, these methods remain fundamentally constrained by *data quality* on two fronts. First, on the *construction side*, reliance on handcrafted augmentations offers limited diversity and risks semantic distortion [67, 78]. Second, on the *learning side*, standard pipelines typically treat all training pairs as equally reliable. This uniform supervision is sub-optimal for noisy web-crawled datasets (e.g., CC12M [9], LAION [63]), where weak alignment can lead to representational degradation.

2.2. Positive Pair Construction

The efficacy of CL hinges on the quality of positive pairs. Approaches generally fall into two categories: recombination-based and generation-based.

Recombination-based Augmentation. Early works focus on task-aware or saliency-preserving augmentations [64, 71]. More recent approaches emphasize multi-view consistency across different spatial or semantic granularities. SwAV [7] introduces a multi-crop strategy that increases the number of views by combining global and local crops without explicit negative samples. VICRegL [4] and LoGo [90] further encourage consistency between global representations and local features, improving transfer performance on dense prediction tasks. A distinct paradigm, such as NNCLR [19] construct positive pairs by retrieving semantically similar samples from the dataset rather than augmenting the instance itself. In the vision-language domain, recombination-based strategies include semantic-preserving perturbations [69] and multimodal mixing or interpolation methods such as MDA [83] and MixGen [27]. Whether using multi-crop or nearest neighbors, these methods are fundamentally bounded by the *original dataset distribution*. They cannot create truly novel visual concepts—such as unseen poses, lighting, or backgrounds—and may retrieve false positives if the dataset

is sparse. This constraint is particularly limiting in VL learning, which demands varied visual contexts for robust grounding.

Generation-based Augmentation. Generative models offer a paradigm shift by synthesizing entirely new views. Early approaches train generators (e.g., GANs) from scratch on the target dataset [3, 41, 68, 84, 87]. However, this is inherently self-limiting as the generator can only interpolate within the seen distribution. Recent work leverages large-scale pretrained diffusion models [62], which encode rich visual priors learned from massive datasets [63]. By injecting this external knowledge, diffusion-based augmentation can synthesize photorealistic views with diverse semantic variations, showing strong potential for representation learning [23, 32, 37, 56, 66, 72, 73, 77, 89]. StableRep [72], for instance, learns invariances by contrasting multiple synthetic images generated from textual prompts. However, existing generative approaches typically lack fine-grained controllability, which often rely on fixed noise levels [32, 72] or randomly sampled ones [66, 73], leading to semantic drift or redundancy across different samples. GenView++ bridges these gaps with a *multi-source adaptive generation* module. We adaptively modulate noise and guidance based on input saliency and complexity, ensuring that the synthesized views are not just new, but optimally balanced for contrastive learning.

2.3. Dynamic Sample Selection and Reweighting

Compounding the construction challenges is the indiscriminate utilization of pairs. Standard pipelines operate on an “augment-and-trust” principle, treating every pair as equally valuable. To address this, extensive research has explored dynamic sample selection. In vision SSL, methods like synthetic hard negatives [17] and hard negative mixing [40] focus on mining informative negative samples. Others propose mining potential positives [16] or reweighting loss to control false negatives [75]. In the VL domain, hardness-weighted mechanisms [39, 43] regulate cross-modal similarity to focus on hard-to-distinguish pairs. While these methods primarily focus on *mining hardness* or *filtering noise* within static datasets, GenView++ tackles a unique problem: assessing the *quality* (fidelity vs. diversity) of synthesized views. Our mechanism explicitly handles the stochastic nature of generative augmentation, rewarding pairs that are both aligned and informative, rather than relying solely on embedding distance.

3. Preliminaries

3.1. Vision Representation Learning

Given a batch of images of size N , for each image \mathbf{I}_i , standard methods generate two augmented views $\mathbf{P}_{i,1} = t_1(\mathbf{I}_i)$ and $\mathbf{P}_{i,2} = t_2(\mathbf{I}_i)$ via random data augmentations $t_1, t_2 \sim$

\mathcal{T} . These are processed by an encoder $\mathcal{E}_{\text{img}}(\cdot)$ and projection head $g(\cdot)$ to obtain representations $\mathbf{v}_{i,1}, \mathbf{v}_{i,2}$. The core goal is to maximize the similarity between these positive views. Most methods (e.g., MoCo [30]) adopt the Noise Contrastive Estimation (NCE) loss:

$$\mathcal{L}_i^{\text{II}} = -\log \frac{\exp(\mathbf{v}_{i,1} \cdot \mathbf{v}_{i,2}/\tau)}{\sum_{k=1}^N \exp(\mathbf{v}_{i,1} \cdot \mathbf{v}_k/\tau)}, \quad (1)$$

where τ is a temperature parameter and \mathbf{v}_k represents features from other samples in the batch. Note that our framework is objective-agnostic and also compatible with non-contrastive losses like the cosine similarity in BYOL [25] or KL-divergence in SwAV [7].

3.2. Vision-Language Representation Learning

Vision–language pretraining aligns images and captions in a shared space. Given a batch of N pairs $\{(\mathbf{I}_i, \mathbf{T}_i)\}$, an image encoder \mathcal{E}_{img} and a text encoder $\mathcal{E}_{\text{text}}$ extract visual features \mathbf{v}_i and textual features \mathbf{t}_i . The standard objective maximizes similarity for matched pairs $(\mathbf{v}_i, \mathbf{t}_i)$ while minimizing it for mismatched ones using a symmetric loss:

$$\mathcal{L}_i^{\text{IT}} = -\log \underbrace{\frac{e^{\langle \mathbf{v}_i, \mathbf{t}_i \rangle / \tau}}{\sum_j e^{\langle \mathbf{v}_i, \mathbf{t}_j \rangle / \tau}}}_{\mathcal{L}_{i,i2t}} - \log \underbrace{\frac{e^{\langle \mathbf{t}_i, \mathbf{v}_i \rangle / \tau}}{\sum_j e^{\langle \mathbf{t}_i, \mathbf{v}_j \rangle / \tau}}}_{\mathcal{L}_{i,t2i}}, \quad (2)$$

where $\langle \cdot, \cdot \rangle$ denotes cosine similarity. GenView++ enhances these objectives by improving the quality of the input positive pairs and reweighting \mathcal{L}^{II} and \mathcal{L}^{IT} .

4. The GenView++ Framework

4.1. Overall Architecture

GenView++ is a unified framework enhancing contrastive learning via two decoupled modules (Fig. 2): **(a) Multi-Source Adaptive View Generation**, an *offline* module that synthesizes diverse, semantically consistent views; and **(b) Quality-Driven Contrastive Learning**, an *online* module that reweights supervision based on pair quality. The framework adapts to two settings:

GenView++ (V): Vision-Only Pretraining. We adopt a *Real-to-Synthetic* strategy. Each real image \mathbf{I}_i is paired with an offline-generated, image-conditioned synthetic view $\mathbf{I}_{i,\text{IC}}$. Unlike utilizing purely synthetic pairs, retaining the real image mitigates feature drift and stabilizes training against generative artifacts. After standard augmentation, the pair $\{\mathbf{P}_{i,\text{ori}}, \mathbf{P}_{i,\text{IC}}\}$ is optimized via the quality-driven image–image loss $\mathcal{L}_i^{\text{II,QD}}$, rewarding foreground consistency and background diversity.

GenView++ (VL): Vision–Language Pretraining. For an image–text pair $(\mathbf{I}_i, \mathbf{T}_i)$, we construct a richer semantic space by expanding the positive set with three offline-generated views: **Image-Conditioned** ($\mathbf{P}_{i,\text{IC}}$), derived

from \mathbf{I}_i to introduce visual diversity while preserving core object semantics. **Text-Conditioned** ($\mathbf{P}_{i,\text{TC}}$), synthesized from \mathbf{T}_i to reflect textual semantics, providing complementary linguistic grounding. **Image–Text-Conditioned** ($\mathbf{P}_{i,\text{ITC}}$), jointly conditioned on \mathbf{I}_i and \mathbf{T}_i to bridge the modality gap with fine-grained control. Combining these with the original augmented view $\mathbf{P}_{i,\text{ori}}$, we obtain the expanded positive set:

$$\mathcal{P}_i = \{\mathbf{P}_{i,\text{ori}}, \mathbf{P}_{i,\text{IC}}, \mathbf{P}_{i,\text{TC}}, \mathbf{P}_{i,\text{ITC}}\}. \quad (3)$$

Training employs two synergistic quality-driven objectives: **Intra-modal Contrast** ($\mathcal{L}_i^{\text{II,QD}}$), which optimizes image pairs within \mathcal{P}_i to learn robustness to visual variations; and **Cross-modal Contrast** ($\mathcal{L}_i^{\text{IT,QD}}$), which aligns each generated view in \mathcal{P}_i with the caption embedding \mathbf{t}_i to ensure semantic grounding.

4.2. Multi-Source Adaptive View Generation

The core innovation of our pair construction is *adaptive controllability*. Instead of applying uniform generation parameters (which risks semantic drift or redundancy), we dynamically modulate the synthesis process for each input. This process is performed offline using a frozen Stable Diffusion model [62], creating a reusable pool of high-quality views without incurring training-time overhead. As shown in Fig. 2 (a), we control the trade-off between fidelity and diversity by adaptively modulating two key hyperparameters:

- **Noise Level** (ℓ): Controls the strength of visual perturbation on the image embedding. Higher ℓ increases structural diversity, while lower ℓ preserves fidelity.
- **Guidance Scale** (g): Controls the adherence to the text prompt. Higher g enforces strict alignment, while lower g fosters creative variation.

Standard formulations for the noise schedule and classifier-free guidance are provided in Appendix 1.1. Below, we detail how we adaptively select these parameters for each generation mode.

4.2.1. Image-Conditioned Adaptive Generation

We detail the calculation of the adaptive noise level ℓ_i^{ada} used to generate $\mathbf{I}_{i,\text{IC}}$. The process consists of foreground estimation followed by noise mapping:

Foreground Proportion Estimation. We estimate the saliency of the main subject $p_i \in [0, 1]$ using a lightweight PCA-based approach. Drawing upon established findings that self-supervised features naturally encode explicit object localization information (e.g., as observed in DINO [8]), we utilize the principal components of feature maps as a robust, training-free foreground proxy. Specifically, we extract dense visual features $\mathbf{F}_i = \mathcal{V}(\mathbf{I}_i) \in \mathbb{R}^{H \times W \times K}$ using the generator’s frozen CLIP image encoder \mathcal{V} . We compute the first principal component $\mathbf{w} \in \mathbb{R}^K$ over a subset

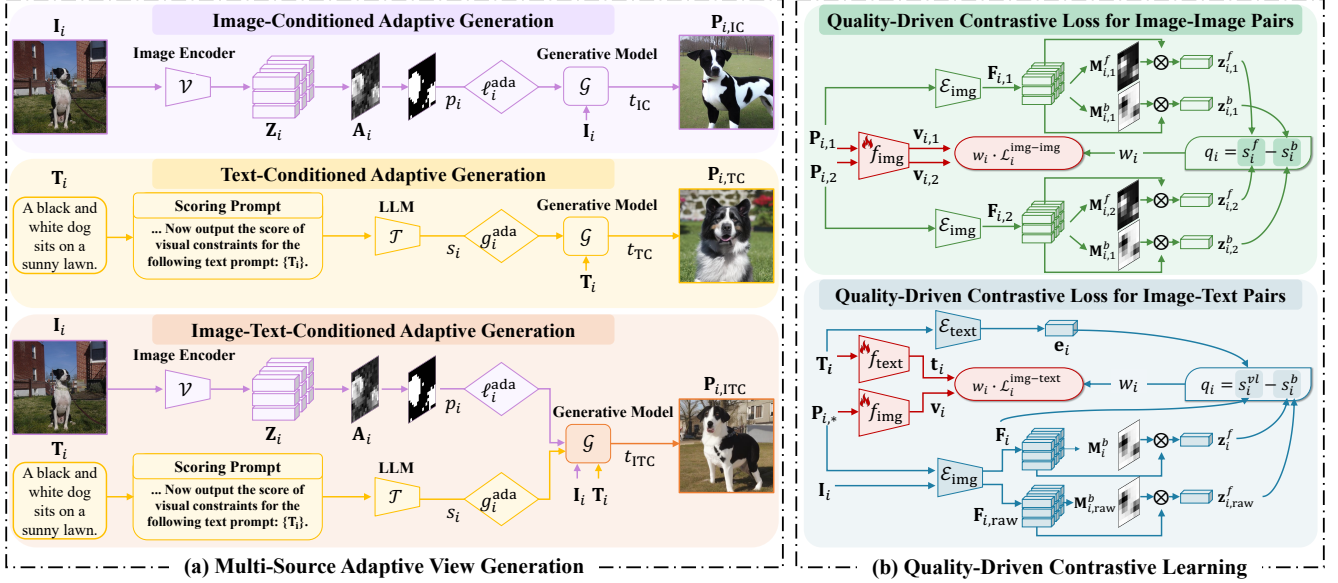


Figure 2. **Overview of GenView++.** (a) **Offline Multi-Source Adaptive View Generation:** Synthesizes diverse views using three strategies: **IC** adjusts noise ℓ by foreground saliency; **TC** adjusts guidance g by caption complexity; **ITC** adapts both. (b) **Online Quality-Driven Contrastive Learning:** Dynamically reweights pairs. High-quality pairs (high alignment, high diversity) receive higher weights w_i , while noisy pairs are suppressed.

of 10,000 training samples. The raw foreground activation map is calculated as $\mathbf{A}_i = \mathbf{F}_i \cdot \mathbf{w}$ and then min-max normalized:

$$\hat{\mathbf{A}}_i = \frac{\mathbf{A}_i - \min(\mathbf{A}_i)}{\max(\mathbf{A}_i) - \min(\mathbf{A}_i)}, \quad \hat{\mathbf{A}}_i \in \mathbb{R}^{H \times W}. \quad (4)$$

The foreground proportion p_i is defined as the ratio of spatial locations exceeding a threshold α :

$$p_i = \frac{1}{HW} \sum_{h=1}^H \sum_{w=1}^W \mathbf{1} \left\{ \hat{\mathbf{A}}_i[h, w] > \alpha \right\}, \quad (5)$$

where $\mathbf{1}\{\cdot\}$ is the indicator function. The threshold α is determined such that approximately 40% of image tokens across the dataset are considered foreground.

Mapping to Adaptive Noise Level. We map the continuous proportion p_i to a discrete noise level ℓ_i^{ada} using a step function:

$$\ell_i^{\text{ada}} = 100 \cdot \left\lfloor \frac{p_i}{0.2} \right\rfloor, \quad \ell_i^{\text{ada}} \in \{0, 100, 200, 300, 400\}. \quad (6)$$

We cap ℓ_i^{ada} at 400 to prevent semantic collapse. Finally, the synthetic view is generated by conditioning the diffusion model \mathcal{G} on the perturbed image embedding:

$$\mathbf{I}_{i,\text{IC}} = \mathcal{G}(\mathbf{z}_i, \text{noisy}(\mathbf{c}_i^{\text{img}}, \ell_i^{\text{ada}})). \quad (7)$$

A random transformation t_{IC} is applied to produce the final view $\mathbf{P}_{i,\text{IC}} = t_{\text{IC}}(\mathbf{I}_{i,\text{IC}})$.

4.2.2. Text-Conditioned Adaptive Generation

We detail the calculation of the adaptive guidance scale g_i^{ada} used to generate $\mathbf{I}_{i,\text{TC}}$. This process ensures that the guidance strength is inversely proportional to the visual complexity of the caption.

Caption Visual Complexity Estimation. We quantify the richness of visual details in caption \mathbf{T}_i into a discrete score $s_i \in \{1, 2, 3, 4\}$. We employ a pretrained language model Φ , prompted with a rule-based scoring instruction $R(\mathbf{T}_i)$ (see Table 13 for the full prompt):

$$s_i = \Phi(R(\mathbf{T}_i)), \quad s_i \in \{1, 2, 3, 4\}. \quad (8)$$

A higher score s_i indicates a caption containing specific constraints (e.g., textures, spatial relations), whereas a lower score indicates abstract or simple descriptions.

Mapping to Adaptive Guidance Scale. We map the complexity score s_i to the guidance scale g_i^{ada} using a linear inverse mapping:

$$g_i^{\text{ada}} = 10 - 2 \cdot s_i, \quad g_i^{\text{ada}} \in \{2, 4, 6, 8\}. \quad (9)$$

This mapping assigns stronger guidance ($g = 8$) to simple captions to prevent semantic drift, and weaker guidance ($g = 2$) to complex captions to encourage diversity. Finally, the synthetic view is generated by conditioning the diffusion model \mathcal{G} on the text embedding $\mathbf{c}_i^{\text{text}}$ using this adaptive scale:

$$\mathbf{I}_{i,\text{TC}} = \mathcal{G}(\mathbf{z}_i, \mathbf{c}_i^{\text{text}}, g_i^{\text{ada}}). \quad (10)$$

A random augmentation t_{TC} is applied to produce the final view $\mathbf{P}_{i,\text{TC}} = t_{\text{TC}}(\mathbf{I}_{i,\text{TC}})$.

4.2.3. Image-Text-Conditioned Adaptive Generation

The ITC mode provides fine-grained cross-modal control by synergistically applying both adaptive strategies defined in the previous sections.

For a given pair $(\mathbf{I}_i, \mathbf{T}_i)$, we compute the adaptive noise level ℓ_i^{ada} based on the image’s foreground proportion (as defined in Eq. 6) and the adaptive guidance scale g_i^{ada} based on the caption’s visual complexity (as defined in Eq. 9).

The synthetic view is generated by conditioning the diffusion model \mathcal{G} on both the perturbed image embedding and the text embedding, utilizing the adaptively selected parameters:

$$\mathbf{I}_{i,\text{ITC}} = \mathcal{G}(\mathbf{z}_i, \text{noisy}(\mathbf{c}_i^{\text{img}}, \ell_i^{\text{ada}}), \mathbf{c}_i^{\text{text}}, g_i^{\text{ada}}). \quad (11)$$

Similar to the other modes, a random transformation t_{ITC} is applied to the synthesized image to produce the final training view $\mathbf{P}_{i,\text{ITC}} = t_{\text{ITC}}(\mathbf{I}_{i,\text{ITC}})$.

4.3. Quality-Driven Contrastive Learning

Existing contrastive frameworks treat all positive pairs equally, which dilutes high-quality supervision. To address this, we introduce *quality-driven contrastive learning*, which replaces uniform supervision with dynamic reweighting. As shown in Fig. 2 (b), an online module evaluates the quality of each image–image or image–text pair and modulates its loss contribution. This module uses a frozen CLIP model as a quality assessor, introducing no trainable parameters.

4.3.1. Quality-Driven Reweighting for Image-Image Pairs

We detail the calculation of the quality weights w_i^{II} for image-image pairs.

Saliency-Guided Feature Decoupling. For a pair of views $(\mathbf{P}_{i,1}, \mathbf{P}_{i,2})$, we extract dense visual representations using the frozen CLIP image encoder $\mathcal{E}_{\text{img}}^*$:

$$\mathbf{F}_{i,1} = \mathcal{E}_{\text{img}}^*(\mathbf{P}_{i,1}), \quad \mathbf{F}_{i,2} = \mathcal{E}_{\text{img}}^*(\mathbf{P}_{i,2}), \quad \mathbf{F} \in \mathbb{R}^{H \times W \times K}. \quad (12)$$

To estimate object attention, we perform PCA on the feature vectors across the channel dimension K . The first principal component is min-max normalized to yield the foreground attention map $\mathbf{M}_{i,1}^f \in [0, 1]^{H \times W}$. The background map is defined as $\mathbf{M}_{i,1}^b = 1 - \mathbf{M}_{i,1}^f$. We apply these maps to decouple the dense features into foreground (\mathbf{z}^f) and background (\mathbf{z}^b) vectors:

$$\begin{aligned} \mathbf{z}_{i,1}^f &= \mathbf{M}_{i,1}^f \otimes \mathbf{F}_{i,1}, & \mathbf{z}_{i,2}^f &= \mathbf{M}_{i,2}^f \otimes \mathbf{F}_{i,2}, \\ \mathbf{z}_{i,1}^b &= \mathbf{M}_{i,1}^b \otimes \mathbf{F}_{i,1}, & \mathbf{z}_{i,2}^b &= \mathbf{M}_{i,2}^b \otimes \mathbf{F}_{i,2}, \end{aligned} \quad (13)$$

where the pooling operation \otimes is defined as $\mathbf{z} = \mathbf{M} \otimes \mathbf{F} = \sum_{h=1}^H \sum_{w=1}^W \mathbf{M}_{h,w} \mathbf{F}_{[h,w,:]}$.

Quality Score Computation. The quality score q_i^{II} is defined as the difference between foreground consistency (s_i^f) and background redundancy (s_i^b):

$$q_i^{\text{II}} = \underbrace{\cos(\mathbf{z}_{i,1}^f, \mathbf{z}_{i,2}^f)}_{s_i^f \text{ (Consistency)}} - \underbrace{\cos(\mathbf{z}_{i,1}^b, \mathbf{z}_{i,2}^b)}_{s_i^b \text{ (Redundancy)}}. \quad (14)$$

Quality-Driven Loss Reweighting. We normalize these scores via softmax to obtain weights w_i^{II} , which modulate the image-image contrastive loss $\mathcal{L}_i^{\text{II}}$:

$$w_i^{\text{II}} = \frac{\exp(q_i^{\text{II}})}{\sum_j \exp(q_j^{\text{II}})}, \quad \mathcal{L}_i^{\text{II, QD}} = w_i^{\text{II}} \cdot \mathcal{L}_i^{\text{II}}. \quad (15)$$

where $\mathcal{L}_i^{\text{II}}$ represents the base objective (e.g., NCE) as defined in the Preliminaries.

4.3.2. Quality-Driven Reweighting for Image-Text Pairs

Extending the quality-driven supervision to the multimodal domain, we evaluate the quality of a generated view $\mathbf{P}_{i,*}$ with respect to its caption \mathbf{T}_i . A high-quality pair should simultaneously exhibit strong *cross-modal semantic alignment* and high *visual novelty* relative to the original image. We formalize this process in three steps.

Multimodal Feature Extraction. We first extract the text embedding \mathbf{e}_i and the dense visual features for both the original image (\mathbf{I}_i) and the generated view ($\mathbf{P}_{i,*}$) using the frozen CLIP encoders $(\mathcal{E}_{\text{text}}^*, \mathcal{E}_{\text{img}}^*)$:

$$\begin{aligned} \mathbf{e}_i &= \mathcal{E}_{\text{text}}^*(\mathbf{T}_i), \quad \mathbf{e}_i \in \mathbb{R}^K, \\ \mathbf{F}_{i,\text{raw}} &= \mathcal{E}_{\text{img}}^*(\mathbf{I}_i), \quad \mathbf{F}_{i,*} = \mathcal{E}_{\text{img}}^*(\mathbf{P}_{i,*}), \quad \mathbf{F} \in \mathbb{R}^{H \times W \times K}. \end{aligned} \quad (16)$$

Using the masking process from Sec. 4.3.1, we obtain background-sensitive vectors:

$$\mathbf{z}_{i,\text{raw}}^b = \mathbf{M}_{i,\text{raw}}^b \otimes \mathbf{F}_{i,\text{raw}}, \quad \mathbf{z}_{i,*}^b = \mathbf{M}_{i,*}^b \otimes \mathbf{F}_{i,*}. \quad (17)$$

Quality Score Computation. We define the quality score based on two criteria: (1) **Alignment** ($s_{i,*}^{\text{IT}}$): Semantic consistency, measured by cosine similarity between text feature \mathbf{e}_i and the pooled image feature. (2) **Redundancy** ($s_{i,*}^b$): Visual redundancy, measured by background similarity between the generated and original view. The final quality score $q_{i,*}^{\text{IT}}$ rewards alignment while penalizing redundancy:

$$q_{i,*}^{\text{IT}} = \underbrace{\cos(\mathbf{e}_i, \text{AvgPool}(\mathbf{F}_{i,*}))}_{s_{i,*}^{\text{IT}} \text{ (Alignment)}} - \underbrace{\cos(\mathbf{z}_{i,\text{raw}}^b, \mathbf{z}_{i,*}^b)}_{s_{i,*}^b \text{ (Redundancy)}}. \quad (18)$$

Quality-Driven Loss Reweighting. We normalize these scores across all positive views in the set \mathcal{P}_i to obtain adaptive weights $w_{i,*}^{\text{IT}}$, which modulate the image-text contrastive loss $\mathcal{L}_i^{\text{IT}}$:

$$w_{i,*}^{\text{IT}} = \frac{\exp(q_{i,*}^{\text{IT}})}{\sum_{j,*} \exp(q_{j,*}^{\text{IT}})}, \quad \mathcal{L}_i^{\text{IT, QD}} = w_{i,*}^{\text{IT}} \cdot \mathcal{L}_i^{\text{IT}}. \quad (19)$$

Table 1. **Linear classification accuracy on ImageNet-1K.** *: our reproduction.

Method	Backbone	Epochs	Top-1
InstDisc [80]	ResNet-50	200	56.5
SimCLR [10]	ResNet-50	200	66.8
PCL [45]	ResNet-50	200	67.6
Adco [59]	ResNet-50	200	68.6
InfoMin [71]	ResNet-50	200	70.1
NNCLR [19]	ResNet-50	200	70.7
LEVEL [36]	ResNet-50	200	72.8
Barlow Twins [88]	ResNet-50	300	71.4
CLIP [60]	ResNet-50	-	74.3
MoCov2 [30]	ResNet-50	200	67.5
MoCov2 + C-Crop [58]	ResNet-50	200	67.8
MoCov2 + GenView++ (V)	ResNet-50	200	70.0
SwAV [7]*	ResNet-50	200	70.5
SwAV + GenView++ (V)	ResNet-50	200	71.7
SimSiam [11]	ResNet-50	200	70.0
SimSiam + GenView++ (V)	ResNet-50	200	72.2
BYOL [25]*	ResNet-50	200	71.8
BYOL + GenView++ (V)	ResNet-50	200	73.2
MoCov3 [13]	ResNet-50	100	68.9
MoCov3 + GenView++ (V)	ResNet-50	100	72.7
MoCov3 [13]	ResNet-50	300	72.8
MoCov3 + GenView++ (V)	ResNet-50	300	74.8
MAE [31]	ViT-B	1600	68.0
I-JEPA [2]	ViT-B	600	72.9
VICReg [4]	CNX-S	400	76.2
DINO [8]*	ViT-S	50	70.3
DINO + GenView++ (V)	ViT-S	50	71.9
MoCov3 [13]	ViT-S	300	73.2
MoCov3 + GenView++ (V)	ViT-S	300	74.5
MoCov3 [13]	ViT-B	300	76.7
MoCov3 + GenView++ (V)	ViT-B	300	77.8

By prioritizing pairs that are both semantically aligned and informative, GenView++ effectively filters out noise and redundancy inherent in generative augmentation.

$$\mathcal{L}_i^{\text{IT},\text{QD}} = w_{i,*}^{\text{IT}} \cdot \mathcal{L}_i^{\text{IT}}. \quad (20)$$

By prioritizing pairs that are both semantically aligned and informative, GenView++ effectively filters out noise and redundancy inherent in generative augmentation.

5. Main Results

5.1. Vision Representation Benchmarks

We integrate GenView++ (V) into six representative SSL frameworks: MoCov2 [30], BYOL [25], DINO [8], SwAV [7], SimSiam [11], and MoCov3 [13]. using ResNet and ViT backbones. Models are pretrained on ImageNet-1K (IN1K). Implementation details are provided in Appendix 2.

Table 2. **Transfer learning performance on MS-COCO for object detection and instance segmentation.** *: our reproduction.

Method	Object Det.			Instance Seg.		
	AP	AP ₅₀	AP ₇₅	AP	AP ₅₀	AP ₇₅
ReSim [82]	39.8	60.2	43.5	36.0	57.1	38.6
DenseCL [76]	40.3	59.9	44.3	36.4	57.0	39.2
SimSiam [11]*	38.5	57.8	42.3	34.7	54.9	37.1
SimSiam + GenView++ (V)	39.1	58.5	43.0	35.2	55.9	37.7
MoCov2 [12]*	39.7	59.4	43.6	35.8	56.5	38.4
MoCov2 + FreeATM [89]	40.1	-	-	-	-	-
MoCov2 + GenView++ (V)	40.5	60.0	44.3	36.3	57.1	38.9
BYOL [25]*	40.6	60.9	44.5	36.7	58.0	39.4
BYOL + GenView++ (V)	41.2	61.5	44.9	37.0	58.4	39.7

5.1.1. Linear Classification

Tab. 1 presents the primary results for linear classification on ImageNet-1K. GenView++ (V) consistently improves the performance of various self-supervised learning (SSL) methods, including both contrastive (e.g., MoCov2, MoCov3) and non-contrastive (e.g., DINO, SimSiam, BYOL, SwAV) approaches. It demonstrates broad applicability and effectiveness with both ResNet and ViT backbones.

GenView++ proves to be highly versatile, showing consistent improvements under different pretraining durations and outperforming MoCov3 baselines at both 100 and 300 epochs. When compared to C-Crop, which also enhances view diversity with advanced handcrafted transformations, GenView++ outperforms it by utilizing a diffusion-based generative augmentation strategy that is not only controllable but also content-aware.

Notably, when combined with MoCov3 (300 epochs), GenView++ achieves a top-1 accuracy of 74.8% on ImageNet-1K, surpassing CLIP (74.3%) trained on 400M image-text pairs. This underscores GenView++’s superior data efficiency and the high quality of the positive pairs it generates.

5.1.2. Transfer to Dense Prediction Tasks

We evaluate transferability on MS-COCO [48] object detection and instance segmentation. As shown in Tab. 2, GenView++ consistently improves both box and mask AP across multiple baselines, demonstrating that our generated views preserve fine-grained spatial information essential for pixel-level tasks. Notably, it achieves higher accuracy than FreeATM [89], which relies on text-prompted augmentation. This confirms that our content-aware, image-conditioned strategy effectively captures visual details for dense prediction even without textual supervision.

5.1.3. Comparison with Dataset Expansion Methods

We evaluate whether GenView++’s performance gains stem merely from increased data volume or from the quality of our adaptive views. We compare GenView++ against

Table 3. Data efficiency analysis on ImageNet-1K. Comparison against external data expansion and naive generation. Note that GenView++ uses only half the number of additional samples compared to baselines yet achieves the best performance.

Dataset	Images	Top-1	Top-5
Baseline (IN1K)	1.28M	62.39	84.57
+ Laion400M	1.28M + 0.3M	63.31	85.53
+ IN21K	1.28M + 0.3M	64.10	85.86
+ Synthetic	1.28M + 0.3M	63.36	85.14
+ GenView++ (V)	1.28M + 0.15M	65.62	87.25

three expansion strategies using MoCo v3 (ResNet-50, 50 epochs) on ImageNet-1K (IN1K):

- **+ Laion400M [63]:** To ensure relevance and minimize domain shift, we use a [retrieval-based technique](#) to select 0.3M images from Laion400M that are most similar to IN1K samples.
- **+ ImageNet-21K (IN21K) [61]:** We randomly sample 0.3M real images with labels matching the IN1K classes.
- **+ Synthetic (Naive):** We generate 0.3M synthetic images without our adaptive noise/guidance control.
- **+ GenView++ (V):** We use only 0.15M adaptively generated views.

Table 3 presents the linear probing results. Expanding with Laion400M or naive synthetic images yields only marginal gains, suggesting that simply adding data—even if retrieved or generated—is inefficient if domain gaps or semantic noise persist. Extending with IN21K brings moderate improvements due to domain proximity. Crucially, GenView++ achieves the highest accuracy (65.62%), outperforming the IN21K expansion by +1.52% despite using 50% fewer added samples (0.15M vs. 0.3M). This result powerfully validates our core premise: *data quality matters more than quantity*. Our adaptive generation strategy constructs highly informative pairs that provide superior supervision compared to large-scale but noisy external data, justifying the one-time offline generation cost with significant data efficiency and performance gains.

5.1.4. Comparison with View Construction Methods

To verify the effectiveness of GenView++ (V) against state-of-the-art positive pair construction methods, we conduct comprehensive pretraining and linear evaluation on CIFAR-10 [42] (CF10), CIFAR-100 [42] (CF100), and Tiny ImageNet [44] (TinyIN). We compare our approach with a wide range of baselines. To facilitate a rigorous comparison, we categorize methods based on the source of data variance they introduce:

- **Within-Instance Variance:** Methods like **Contrastive-Crop (C-Crop) [58]** optimize geometric transformations (e.g., cropping) based on the information within a single image.

Table 4. Linear classification results of view construction methods on CIFAR-10, CIFAR-100, and TinyImageNet.

Method	CF10	CF100	TinyIN
<i>Variance within instance</i>			
MoCov2 + C-Crop [58]	88.78	57.65	47.98
BYOL + C-Crop [58]	92.54	64.62	47.23
<i>Variance within pretraining datasets</i>			
SimCLR + ViewMaker [68]	86.30	-	-
SimCLR + NTN [41]	86.90	-	-
MoCov2 + LMA [84]	92.02	64.89	-
SimSiam + LMA [84]	92.46	65.70	-
Simsiam + DiffAug [87]	87.30	60.10	45.30
<i>Variance beyond pretraining datasets</i>			
W-perturb [26]	92.90	-	51.05
MoCov2 + GenView++ (V)	93.00	67.49	56.76
BYOL + GenView++ (V)	93.56	67.53	54.79

- **Within-Dataset Variance:** Methods such as **View-Maker [68]**, **Neural Transform Network (NTN) [41]**, and **Local Manifold Augmentation (LMA) [84]** synthesize new views by learning from the existing dataset distribution (e.g., via mixup or learned perturbations).
- **Beyond-Dataset Variance:** Methods like **DiffAug [87]** and **W-perturb [26]** introduce additional semantic diversity leveraging external generative models or perturbation functions. GenView++ falls into this category but introduces adaptive controllability.

We strictly follow the standard evaluation protocols for small-scale datasets to ensure fair comparison. Table 4 presents the comparative results. GenView++ (V) yields consistent improvements across all datasets:

Superiority over Internal Methods: GenView++ significantly outperforms methods relying on internal variance (e.g., C-Crop, LMA). For instance, on CIFAR-100, MoCov2 + GenView++ surpasses MoCov2 + LMA by **+2.60%** (67.49% vs. 64.89%). This confirms that injecting rich, external visual knowledge via pretrained diffusion models provides more discriminative signals than merely manipulating dataset statistics.

Advantage of Adaptive Controllability: Crucially, GenView++ outperforms other generative approaches like W-perturb (e.g., **+5.71%** on TinyIN). While standard generative methods introduce diversity, they often lack control. Our saliency-guided adaptive strategy ensures that the generated views maintain high semantic fidelity, preventing the noise injection (common in DiffAug or W-perturb) from corrupting the representation learning process.

5.2. Vision-Language Representation Benchmarks

We evaluate GenView++ (VL) on linear probing, zero-shot classification, and cross-modal retrieval. We use a ViT-B/16

Table 5. **Linear classification accuracy on visual benchmarks.** “I-I” and “I-T” indicate the number of image-image and image-text pairs used. StableRep results are reproduced by us with official weights.

Method	Venue	I-I	I-T	IN1K	CF10	CF100	Aircraft	DTD	Flowers	Pets	SUN397	Caltech-101	Food-101	Avg.
CLIP [60]	ICML’21	0	1	53.30	81.80	62.70	34.70	57.30	84.10	60.50	54.30	75.60	58.70	62.30
GenView++ (VL)	-	0	1	60.49	92.24	76.08	35.01	64.47	86.18	69.96	62.41	92.45	68.24	70.75
StableRep [72]	NeurIPS’23	6	0	63.86	93.03	76.02	29.19	69.84	83.53	70.51	65.53	90.67	70.91	71.31
GenView++ (VL)	-	6	0	64.38	93.53	77.33	32.64	69.15	86.86	73.04	65.77	91.47	72.39	72.66
SLIP [51]	ECCV’22	1	1	65.40	-	-	-	-	-	-	-	-	-	-
GenView++ (VL)	-	1	1	66.44	94.53	79.23	38.46	69.47	87.06	75.88	67.43	91.99	74.13	74.46
GenView++ (VL)	-	6	4	68.17	95.08	80.26	40.23	71.17	90.00	77.46	69.03	92.22	75.96	75.96

Table 6. **Zero-shot classification results on various downstream datasets.** Results for CLIP, SLIP, and TripletCLIP are reproduced by us using their official pretrained weights.

Method	Venue	IN1K	CF10	CF100	Aircraft	DTD	Flowers	Pets	SUN397	Caltech-101	Food-101	Avg.
CLIP [60]	ICML’21	16.34	41.10	17.42	1.11	11.49	10.25	11.37	32.17	49.66	10.73	20.16
SLIP [51]	ECCV’22	23.00	64.38	33.61	1.23	13.19	13.58	16.68	33.00	58.16	14.77	27.16
LaCLIP [21]	NeurIPS’23	21.50	57.10	27.50	1.60	16.60	14.70	15.60	35.10	52.70	14.20	25.66
TripletCLIP [56]	NeurIPS’24	7.00	25.26	12.51	1.29	10.69	6.34	5.51	14.78	31.54	4.84	5.09
GenView++ (VL)	-	23.16	87.82	50.64	1.59	19.10	12.50	12.73	42.44	60.63	14.07	32.47

Table 7. **Zero-shot cross-modal retrieval performance on MS COCO, Flickr30k, and Flickr8k.** We report Recall@1 (R@1) and Recall@5 (R@5) for Text-to-Image and Image-to-Text retrieval. CLIP and SLIP results are reproduced by us.

Method	Venue	MS Coco				Flickr30k				Flickr8k	
		Text→Image		Image→Text		Text→Image		Image→Text		Text→Image	Image→Text
		R@1	R@5	R@1	R@5	R@1	R@5	R@1	R@5	R@1	R@1
CLIP [60]	ICML’21	9.80	25.78	13.40	31.00	19.12	41.32	25.80	54.50	20.00	29.00
SLIP [51]	ECCV’22	15.25	34.87	20.60	43.88	27.74	51.48	36.90	63.80	28.36	40.10
TripletCLIP [56]	NeurIPS’24	-	11.28	-	10.38	-	22.00	-	22.00	-	-
GenView++ (VL)	-	16.12	36.80	20.12	45.02	28.16	54.82	38.20	67.00	29.08	41.10

backbone pretrained on CC3M (partially enhanced by our adaptive generation) following StableRep [72] protocols. Full training details are provided in Appendix 2.2.

5.2.1. Linear Classification

Tab. 5 reports linear probing accuracy across 10 benchmarks.

Vision-Language Setting (0 I-I, 1 I-T): To ensure a strictly fair comparison with CLIP, this setting restricts the input to a single image-text pair per sample, matching CLIP’s exact computational budget per iteration. Remarkably, even under this identical view constraint, GenView++ achieves an average accuracy of **70.75%**, surpassing CLIP (62.30%) by a substantial **+8.45%**. This result is critical: it conclusively proves that our performance gains stem from the superior *quality* of our adaptive view construction and reweighting mechanism, rather than merely from increasing the number of training views or data throughput.

Vision-only Setting (6 I-I, 0 I-T): We utilize image-image pairs from our generated pool without text supervision. Compared to StableRep, which also trains on multi-view synthetic data (text-to-image), GenView++ performs

better on 9 of 10 datasets. Notably, it excels in fine-grained categories like Aircraft (**+3.45%**). This confirms that our *multi-source* strategy—specifically the inclusion of Image-Conditioned views—preserves fine-grained object semantics better than text-only synthesis, while our quality-driven loss effectively filters generative noise.

Unified Synergy & Performance Upper Bound (Full GenView++): Finally, we explore the performance ceiling of our framework by combining all generated views (6 I-I, 4 I-T). While this setting incurs a higher computational cost per iteration, it yields state-of-the-art results, reaching **68.17%** on IN1K and **75.96%** on Food-101. This empirically demonstrates the upper bound of our method, validating that when computational resources permit, the synergistic alignment of intra-modal and cross-modal representations can drive representation quality to new heights.

5.2.2. Zero-Shot Classification

Tab. 6 reports zero-shot performance across 10 benchmarks. GenView++ achieves an average top-1 accuracy of **32.47%**, significantly outperforming CLIP (**+12.31%**), SLIP (**+5.31%**), and LaCLIP (**+6.81%**). Notably, we

Table 8. **Effect of core components in GenView++ (V) under linear evaluation on IN100.** “Our framework” denotes real-to-synthetic view construction without adaptive noise control or quality-driven loss. “AdaGen” refers to adaptive image-conditioned view generation. “Qual.Driv.Cont” indicates the use of quality-driven contrastive loss.

Our framework	AdaGen	Qual.Driv.Cont	Top-1
×	×	×	65.52
×	×	✓	66.97 (↑ 1.45)
✓	×	×	71.50 (↑ 5.98)
✓	✓	×	73.96 (↑ 8.44)
✓	×	✓	74.88 (↑ 9.36)
✓	✓	✓	75.40 (↑ 9.88)

achieve strong results on general-purpose datasets (e.g., **87.82%** on CIFAR-10), demonstrating robust transferability. Unlike methods such as TripletCLIP [56] that rely on hard negative mining, GenView++ focuses on constructing high-quality *positive* views. By generating semantically consistent yet diverse positives, our framework not only strengthens the alignment signal but also implicitly enriches the negative pool with informative hard negatives. Coupled with quality-driven supervision, we achieve stable cross-modal alignment and superior downstream generalization

5.2.3. Zero-Shot Cross-Modal Retrieval

Tab. 7 reports the zero-shot text-to-image and image-to-text retrieval results on MS COCO [48], Flickr30k [86], and Flickr8k [35]. On Flickr30k Image-to-Text retrieval (R@5), it surpasses SLIP by **+3.20%** and CLIP by **+12.50%**. Consistent gains are also observed on MS COCO (e.g., **+1.93%** Text-to-Image R@5 over SLIP). These results confirm that our quality-driven contrastive loss effectively aligns the visual and textual embedding spaces, facilitating cross-modal matching even without task-specific fine-tuning.

6. Ablation Studies and Analysis

6.1. Vision Component Ablation

We analyze the contribution of each unimodal component using ResNet-18 on ImageNet-100. Tab. 8 shows that the base generative framework (Real-to-Synthetic pairing) alone yields a significant **+5.98%** gain. Refining this with **Adaptive Generation (AdaGen)** boosts accuracy to 73.96% (**+8.44%** over baseline), validating the importance of saliency-aware noise modulation. Finally, integrating **Quality-Driven Contrastive Learning** achieves the best performance (**75.40%**, **+9.88%** total gain), demonstrating the strong synergy between controllable view synthesis and quality-aware supervision.

6.2. Vision-Language Component Ablation

We analyze multimodal components using ViT-B/16 pre-trained on a 1M subset of CC3M, with enhancements from

Table 9. **Effectiveness of multi-source adaptive generation.** We compare different generation sources (IC, TC, ITC) and the effect of our adaptive strategy (AdaGen).

Generation Setting				500k Aug.		100k Aug.	
IC	TC	ITC	AdaGen	CF10	IN100	CF10	IN100
×	×	×	×	83.41	66.76	83.41	66.76
✓	×	×	×	86.98	72.96	85.17	68.98
✓	×	×	✓	88.05	76.50	86.02	71.54
×	✓	×	×	87.55	72.60	84.84	69.14
×	✓	×	✓	88.99	75.26	85.62	70.86
×	×	✓	×	87.39	72.86	84.40	68.92
×	×	✓	✓	88.60	76.38	85.45	71.40
✓	✓	✓	✓	90.69	78.38	87.61	74.28

Table 10. **Effectiveness of quality-driven contrastive learning.** “Qual.Driv.Cont” denotes quality-driven loss, and “Lang.Sup” denotes the image-text contrastive loss.

Qual.Driv.Cont	Lang.Sup	500k Aug.		100k Aug.	
		CF10	IN100	CF10	IN100
×	×	90.69	78.38	87.61	74.28
✓	×	91.61	79.58	90.77	78.10
×	✓	92.03	80.04	91.98	79.64
✓	✓	92.85	81.38	92.72	80.56

our adaptive view generation module. Performance is evaluated with linear probe top-1 accuracy on CIFAR-10 and ImageNet-100. Full details are in Appendix 2.4.

6.2.1. Effectiveness of Multi-Source Adaptive Generation

Tab. 9 validates the contribution of our generation strategies. Introducing any single generative source (IC, TC, or ITC in Rows 2, 4, 6) provides gains over the baseline (Row 1). For example, IC-only at the 500k setting boosts IN100 by **+6.20%** (Row 2), demonstrating the value of generative diversity in enhancing representation quality. Enabling **Adaptive Generation (AdaGen)** consistently improves performance across all modes. For IC at 500k, AdaGen increases IN100 from **72.96% to 76.50%** (+3.54%, Row 3). Similar gains are observed for TC (+2.66%, Row 5) and ITC (+3.52%, Row 7), confirming that our content-aware control produces more reliable and informative views. The synergy of all three modes with AdaGen achieves the best results, reaching **90.69%** (CF10) and **78.38%** (IN100) at 500k (Row 8), and **87.61% / 74.28%** at 100k. This demonstrates that combining image-conditioned visual structure with text-conditioned semantic grounding yields a significantly richer representation space than single-source alternatives.

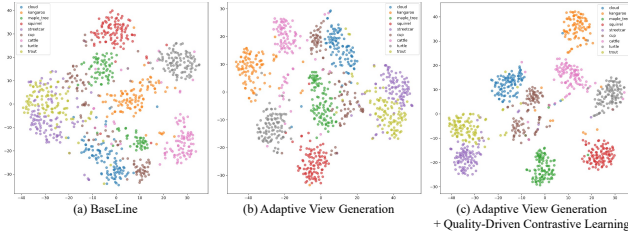


Figure 3. **T-SNE visualization of image features from 9 randomly selected CIFAR-100 classes.** (a) Baseline with standard augmentations; (b) model with multi-source adaptive view generation; (c) full GenView++ with the additional quality-driven contrastive loss.

6.2.2. Effectiveness of Quality-Driven Contrastive Learning

Tab. 10 reports the effect of our quality-driven contrastive loss: **In the vision-only setting** (no text supervision), incorporating quality-driven loss boosts IN100 accuracy by **+3.82%** (Row 2 vs. 1), proving its ability to filter noisy image pairs. Crucially, this advantage persists **in the vision-language setting** (**+1.34%**, Row 4 vs. 3), demonstrating the value of prioritizing high-quality pairs in refining the training signal for both unimodal and multimodal learning.

6.2.3. Impact of Generative Augmentation Ratio

We observe a consistent positive correlation between the volume of synthetic data and performance across Tables 9 and 10. For instance, increasing the synthetic view budget from 100k to 500k yields a further **+0.82%** gain (Tab. 10, Row 4). This confirms that larger amounts of high-quality generative data consistently enhance downstream performance, validating the scalability of our framework.

6.3. Qualitative Analysis

To visualize the learned embedding space, Figure 3 presents t-SNE plots for 9 randomly selected CIFAR-100 classes. **(a) Baseline:** Standard augmentations result in diffuse, overlapping clusters, indicating poor inter-class separability. **(b) +Adaptive Views:** Incorporating multi-source adaptive generation produces distinct, well-separated clusters, confirming that diverse yet semantically consistent views enhance discrimination. **(c) Full GenView++:** Adding the quality-driven loss further compresses intra-class variance and sharpens boundaries. This visually validates the synergy between controlled generation and quality-aware supervision in shaping a robust feature space.

7. Conclusion

We introduced GenView++, a unified framework that enhances contrastive learning by jointly optimizing the construction and utilization of positive pairs. To overcome the limitations of handcrafted and generative augmentations, our multi-source adaptive view generation module

leverages image, text, and joint conditioning to synthesize diverse yet semantically consistent views. Complementing this, our quality-driven contrastive learning mechanism explicitly assesses pair alignment and diversity, dynamically reweighting the loss to prioritize informative supervision while suppressing noise. Both components are model-agnostic and highly efficient: the generation process creates a reusable view pool without training overhead, and the reweighting mechanism is lightweight. Extensive experiments demonstrate that GenView++ consistently outperforms strong baselines across both vision-only and vision-language benchmarks. By effectively bridging controllable generation with quality-aware supervision, GenView++ provides a robust and scalable foundation for future data-centric representation learning.

References

- [1] Yuki M. Asano, Christian Rupprecht, and Andrea Vedaldi. Self-labelling via simultaneous clustering and representation learning. In *ICLR*, 2020. 3
- [2] Mahmoud Assran, Quentin Duval, Ishan Misra, Piotr Bojanowski, Pascal Vincent, Michael Rabbat, Yann LeCun, and Nicolas Ballas. Self-supervised learning from images with a joint-embedding predictive architecture. In *CVPR*, 2023. 3, 7
- [3] Pietro Astolfi, Arantxa Casanova, Jakob Verbeek, Pascal Vincent, Adriana Romero-Soriano, and Michal Drozdal. Instance-conditioned gan data augmentation for representation learning. *arXiv:2303.09677*, 2023. 3
- [4] Adrien Bardes, Jean Ponce, and Yann LeCun. Vicregl: Self-supervised learning of local visual features. In *NeurIPS*, 2022. 3, 7
- [5] Lukas Bossard, Matthieu Guillaumin, and Luc Van Gool. Food-101—mining discriminative components with random forests. In *ECCV*, 2014. 2
- [6] Mathilde Caron, Piotr Bojanowski, Armand Joulin, and Matthijs Douze. Deep clustering for unsupervised learning of visual features. In *ECCV*, 2018. 3
- [7] Mathilde Caron, Ishan Misra, Julien Mairal, Priya Goyal, Piotr Bojanowski, and Armand Joulin. Unsupervised learning of visual features by contrasting cluster assignments. In *NeurIPS*, 2020. 1, 3, 4, 7
- [8] Mathilde Caron, Hugo Touvron, Ishan Misra, Hervé Jégou, Julien Mairal, Piotr Bojanowski, and Armand Joulin. Emerging properties in self-supervised vision transformers. In *ICCV*, 2021. 4, 7
- [9] Soravit Changpinyo, Piyush Sharma, Nan Ding, and Radu Soricut. Conceptual 12m: Pushing web-scale image-text pre-training to recognize long-tail visual concepts. In *CVPR*, 2021. 3
- [10] Ting Chen, Simon Kornblith, Mohammad Norouzi, and Geoffrey Hinton. A simple framework for contrastive learning of visual representations. In *ICML*, 2020. 1, 3, 7
- [11] Xinlei Chen and Kaiming He. Exploring simple siamese representation learning. In *CVPR*, 2021. 3, 7

- [12] Xinlei Chen, Haoqi Fan, Ross Girshick, and Kaiming He. Improved baselines with momentum contrastive learning. In *arXiv:2003.04297*, 2020. 3, 7
- [13] Xinlei Chen, Saining Xie, and Kaiming He. An empirical study of training self-supervised vision transformers. In *ICCV*, 2021. 7
- [14] Mircea Cimpoi, Subhansu Maji, Iasonas Kokkinos, Sammy Mohamed, and Andrea Vedaldi. Describing textures in the wild. In *CV[R]*, 2014. 2
- [15] Jia Deng, Wei Dong, Richard Socher, Li-Jia Li, Kai Li, and Li Fei-Fei. Imagenet: A large-scale hierarchical image database. In *CVPR*, 2009. 1, 2
- [16] Hengkui Dong, Xianzhong Long, and Yun Li. Rethinking samples selection for contrastive learning: Mining of potential samples. *Knowledge-Based Systems*, 2024. 3
- [17] Hengkui Dong, Xianzhong Long, and Yun Li. Synthetic hard negative samples for contrastive learning. *Neural Processing Letters*, 2024. 3
- [18] Alexey Dosovitskiy, Lucas Beyer, Alexander Kolesnikov, Dirk Weissenborn, Xiaohua Zhai, Thomas Unterthiner, Mostafa Dehghani, Matthias Minderer, Georg Heigold, Sylvain Gelly, et al. An image is worth 16x16 words: transformers for image recognition at scale. In *ICLR*, 2020. 1
- [19] Debidatta Dwibedi, Yusuf Aytar, Jonathan Tompson, Pierre Sermanet, and Andrew Zisserman. With a little help from my friends: Nearest-neighbor contrastive learning of visual representations. In *ICCV*, 2021. 3, 7
- [20] Aleksandr Ermolov, Aliaksandr Siarohin, Enver Sangineto, and Nicu Sebe. Whitenig for self-supervised representation learning. In *ICML*, 2021. 3
- [21] Lijie Fan, Dilip Krishnan, Phillip Isola, Dina Katabi, and Yonglong Tian. Improving clip training with language rewrites. *NeurIPS*, 2023. 9
- [22] Li Fei-Fei, Rob Fergus, and Pietro Perona. Learning generative visual models from few training examples: An incremental bayesian approach tested on 101 object categories. In *CVPR Workshop*, 2004. 2
- [23] Yunxiang Fu, Chaoqi Chen, Yu Qiao, and Yizhou Yu. Dreamda: Generative data augmentation with diffusion models. *arXiv:2403.12803*, 2024. 3
- [24] Spyros Gidaris, Praveer Singh, and Nikos Komodakis. Unsupervised representation learning by predicting image rotations. In *ICLR*, 2018. 3
- [25] Jean-Bastien Grill, Florian Strub, Florent Altché, Corentin Tallec, Pierre Richemond, Elena Buchatskaya, Carl Doersch, Bernardo Avila Pires, Zhaohan Guo, Mohammad Gheshlaghi Azar, et al. Bootstrap your own latent: A new approach to self-supervised learning. In *NeurIPS*, 2020. 1, 3, 4, 7
- [26] Ligong Han, Seungwook Han, Shivchander Sudalairaj, Charlotte Loh, Rumen Dangovski, Fei Deng, Pulkit Agrawal, Dimitris Metaxas, Leonid Karlinsky, Tsui-Wei Weng, et al. Constructive assimilation: Boosting contrastive learning performance through view generation strategies. *arXiv:2304.00601*, 2023. 8
- [27] Xiaoshuai Hao, Yi Zhu, Srikar Appalaraju, Aston Zhang, Wanqian Zhang, Bo Li, and Mu Li. Mixgen: A new multi-modal data augmentation. In *WACV*, 2023. 3
- [28] Kaiming He, Xiangyu Zhang, Shaoqing Ren, and Jian Sun. Deep residual learning for image recognition. In *CVPR*, 2016. 1
- [29] Kaiming He, Georgia Gkioxari, Piotr Dollár, and Ross Girshick. Mask r-cnn. In *ICCV*, 2017. 2
- [30] Kaiming He, Haoqi Fan, Yuxin Wu, Saining Xie, and Ross Girshick. Momentum contrast for unsupervised visual representation learning. In *CVPR*, 2020. 1, 3, 4, 7
- [31] Kaiming He, Xinlei Chen, Saining Xie, Yanghao Li, Piotr Dollár, and Ross Girshick. Masked autoencoders are scalable vision learners. In *CVPR*, 2022. 1, 3, 7
- [32] Ruifei He, Shuyang Sun, Xin Yu, Chuhui Xue, Wenqing Zhang, Philip Torr, Song Bai, and Xiaojuan Qi. Is synthetic data from generative models ready for image recognition? In *ICLR*, 2022. 3
- [33] Jonathan Ho and Tim Salimans. Classifier-free diffusion guidance. In *NeurIPS*, 2022. 1
- [34] Jonathan Ho, Ajay Jain, and Pieter Abbeel. Denoising diffusion probabilistic models. In *NeurIPS*, 2020. 1
- [35] Micah Hodosh, Peter Young, and Julia Hockenmaier. Framing image description as a ranking task: Data, models and evaluation metrics. *JAIR*, 2013. 10, 2
- [36] Lang Huang, Shan You, Mingkai Zheng, Fei Wang, Chen Qian, and Toshihiko Yamasaki. Learning where to learn in cross-view self-supervised learning. In *CVPR*, 2022. 7
- [37] Ali Jahanian, Xavier Puig, Yonglong Tian, and Phillip Isola. Generative models as a data source for multiview representation learning. In *ICLR*, 2021. 3
- [38] Chao Jia, Yinfei Yang, Ye Xia, Yi-Ting Chen, Zarana Parekh, Hieu Pham, Quoc Le, Yun-Hsuan Sung, Zhen Li, and Tom Duerig. Scaling up visual and vision-language representation learning with noisy text supervision. In *ICML*, 2021. 3
- [39] Chaoya Jiang, Wei Ye, Haiyang Xu, Songfang Huang, Fei Huang, and Shikun Zhang. Vision language pre-training by contrastive learning with cross-modal similarity regulation. In *ACL*, 2023. 3
- [40] Yannis Kalantidis, Mert Bulent Sariyildiz, Noe Pion, Philippe Weinzaepfel, and Diane Larlus. Hard negative mixing for contrastive learning. In *NeurIPS*, 2020. 3
- [41] Taekyung Kim, Debasmit Das, Seokeon Choi, Minki Jeong, Seunghan Yang, Sungrack Yun, and Changick Kim. Neural transformation network to generate diverse views for contrastive learning. In *CVPR*, 2023. 3, 8
- [42] Alex Krizhevsky, Geoffrey Hinton, et al. Learning multiple layers of features from tiny images. 2009. 8, 2
- [43] Zhibin Lan, Liqiang Niu, Fandong Meng, Jie Zhou, and Jinsong Su. Llave: Large language and vision embedding models with hardness-weighted contrastive learning. *arXiv preprint arXiv:2503.04812*, 2025. 3
- [44] Ya Le and Xuan Yang. Tiny imagenet visual recognition challenge. In *CS 231N*, 2015. 8
- [45] Junnan Li, Pan Zhou, Caiming Xiong, Richard Socher, and Steven CH Hoi. Prototypical contrastive learning of unsupervised representations. In *ICLR*, 2020. 3, 7
- [46] Junnan Li, Dongxu Li, Caiming Xiong, and Steven Hoi. Blip: Bootstrapping language-image pre-training for unified vision-language understanding and generation. In *ICML*, 2022. 1, 3

- [47] Xiaojie Li, Yibo Yang, Xiangtai Li, Jianlong Wu, Yue Yu, Bernard Ghanem, and Min Zhang. Genview: Enhancing view quality with pretrained generative model for self-supervised learning. In *ECCV*, 2024. 2
- [48] Tsung-Yi Lin, Michael Maire, Serge Belongie, James Hays, Pietro Perona, Deva Ramanan, Piotr Dollár, and C Lawrence Zitnick. Microsoft coco: common objects in context. In *ECCV*, 2014. 7, 10, 2
- [49] Ilya Loshchilov and Frank Hutter. SGDR: Stochastic gradient descent with warm restarts. In *ICLR*, 2017. 2
- [50] Subhransu Maji, Esa Rahtu, Juho Kannala, Matthew Blaschko, and Andrea Vedaldi. Fine-grained visual classification of aircraft. *arXiv:1306.5151*, 2013. 2
- [51] Norman Mu, Alexander Kirillov, David Wagner, and Saining Xie. Slip: Self-supervision meets language-image pre-training. In *ECCV*, 2022. 9
- [52] Maria-Elena Nilsback and Andrew Zisserman. Automated flower classification over a large number of classes. In *ICVGIP*, 2008. 2
- [53] Mehdi Noroozi and Paolo Favaro. Unsupervised learning of visual representations by solving jigsaw puzzles. In *ECCV*, 2016. 3
- [54] Aaron van den Oord, Yazhe Li, and Oriol Vinyals. Representation learning with contrastive predictive coding. *arXiv:1807.03748*, 2018. 3
- [55] Omkar M Parkhi, Andrea Vedaldi, Andrew Zisserman, and CV Jawahar. Cats and dogs. In *CVPR*, 2012. 2
- [56] Maitreya Patel, Naga Sai Abhiram Kusumba, Sheng Cheng, Changhoon Kim, Tejas Gokhale, Chitta Baral, et al. Triplet-clip: Improving compositional reasoning of clip via synthetic vision-language negatives. In *NeurIPS*, 2024. 3, 9, 10
- [57] Deepak Pathak, Philipp Krahenbuhl, Jeff Donahue, Trevor Darrell, and Alexei A Efros. Context encoders: Feature learning by inpainting. In *CVPR*, 2016. 3
- [58] Xiangyu Peng, Kai Wang, Zheng Zhu, Mang Wang, and Yang You. Crafting better contrastive views for siamese representation learning. In *CVPR*, 2022. 7, 8
- [59] Guo-Jun Qi, Liheng Zhang, Feng Lin, and Xiao Wang. Learning generalized transformation equivariant representations via autoencoding transformations. *TPAMI*, 2020. 7
- [60] Alec Radford, Jong Wook Kim, Chris Hallacy, Aditya Ramesh, Gabriel Goh, Sandhini Agarwal, Girish Sastry, Amanda Askell, Pamela Mishkin, Jack Clark, et al. Learning transferable visual models from natural language supervision. In *ICML*, 2021. 1, 3, 7, 9
- [61] Tal Ridnik, Emanuel Ben-Baruch, Asaf Noy, and Lih Zelnik-Manor. Imagenet-21k pretraining for the masses. *arXiv:2104.10972*, 2021. 8
- [62] Robin Rombach, Andreas Blattmann, Dominik Lorenz, Patrick Esser, and Björn Ommer. High-resolution image synthesis with latent diffusion models. In *CVPR*, 2022. 1, 3, 4
- [63] Christoph Schuhmann, Romain Beaumont, Richard Vencu, Cade Gordon, Ross Wightman, Mehdi Cherti, Theo Coombes, Aarush Katta, Clayton Mullis, Mitchell Wortsman, et al. Laion-5b: An open large-scale dataset for training next generation image-text models. In *NeurIPS*, 2022. 2, 3, 8
- [64] Ramprasaath R Selvaraju, Karan Desai, Justin Johnson, and Nikhil Naik. Casting your model: Learning to localize improves self-supervised representations. In *CVPR*, 2021. 3
- [65] Piyush Sharma, Nan Ding, Sebastian Goodman, and Radu Soricut. Conceptual captions: A cleaned, hypernymed, image alt-text dataset for automatic image captioning. In *ACL*, 2018. 2, 1
- [66] Jordan Shipard, Arnold Wiliem, Kien Nguyen Thanh, Wei Xiang, and Clinton Fookes. Diversity is definitely needed: Improving model-agnostic zero-shot classification via stable diffusion. In *CVPR*, 2023. 3
- [67] Connor Shorten and Taghi M Khoshgoftaar. A survey on image data augmentation for deep learning. *Journal of Big Data*, 2019. 3
- [68] Alex Tamkin, Mike Wu, and Noah Goodman. Viewmaker networks: Learning views for unsupervised representation learning. In *ICLR*, 2020. 3, 8
- [69] Ruixue Tang, Chao Ma, Wei Emma Zhang, Qi Wu, and Xiaokang Yang. Semantic equivalent adversarial data augmentation for visual question answering. In *ECCV*, 2020. 3
- [70] Yonglong Tian, Dilip Krishnan, and Phillip Isola. Contrastive multiview coding. In *ECCV*, 2020. 3, 2
- [71] Yonglong Tian, Chen Sun, Ben Poole, Dilip Krishnan, Cordelia Schmid, and Phillip Isola. What makes for good views for contrastive learning? In *NeurIPS*, 2020. 3, 7
- [72] Yonglong Tian, Lijie Fan, Phillip Isola, Huiwen Chang, and Dilip Krishnan. Stablerep: Synthetic images from text-to-image models make strong visual representation learners. In *NeurIPS*, 2023. 1, 3, 9, 2
- [73] Brandon Trabucco, Kyle Doherty, Max Gurinas, and Ruslan Salakhutdinov. Effective data augmentation with diffusion models. In *ICLR*, 2023. 3
- [74] Pascal Vincent, Hugo Larochelle, Yoshua Bengio, and Pierre-Antoine Manzagol. Extracting and composing robust features with denoising autoencoders. In *ICML*, 2008. 3
- [75] Tianqi Wang, Lei Chen, Xiaodan Zhu, Younghun Lee, and Jing Gao. Weighted contrastive learning with false negative control to help long-tailed product classification. In *ACL*, 2023. 3
- [76] Xinlong Wang, Rufeng Zhang, Chunhua Shen, Tao Kong, and Lei Li. Dense contrastive learning for self-supervised visual pre-training. In *CVPR*, 2021. 7
- [77] Zhicai Wang, Longhui Wei, Tan Wang, Heyu Chen, Yanbin Hao, Xiang Wang, Xiangnan He, and Qi Tian. Enhance image classification via inter-class image mixup with diffusion model. In *CVPR*, 2024. 3
- [78] Jason Wei and Kai Zou. Eda: Easy data augmentation techniques for boosting performance on text classification tasks. In *EMNLP*, 2019. 3
- [79] Yuxin Wu, Alexander Kirillov, Francisco Massa, Wan-Yen Lo, and Ross Girshick. Detectron2. 2019. 2
- [80] Zhirong Wu, Yuanjun Xiong, Stella X Yu, and Dahua Lin. Unsupervised feature learning via non-parametric instance discrimination. In *CVPR*, 2018. 3, 7
- [81] Jianxiong Xiao, James Hays, Krista A Ehinger, Aude Oliva, and Antonio Torralba. Sun database: Large-scale scene recognition from abbey to zoo. In *CVPR*, 2010. 2

- [82] Tete Xiao, Colorado J Reed, Xiaolong Wang, Kurt Keutzer, and Trevor Darrell. Region similarity representation learning. In *ICCV*, 2021. 7
- [83] Nan Xu, Wenji Mao, Penghui Wei, and Daniel Zeng. Mda: Multimodal data augmentation framework for boosting performance on sentiment/emotion classification tasks. *IEEE Intell. Syst.*, 2020. 3
- [84] Yu Yang, Wing Yin Cheung, Chang Liu, and Xiangyang Ji. Local manifold augmentation for multiview semantic consistency. *arXiv:2211.02798*, 2022. 3, 8
- [85] Moon Ye-Bin, Nam Hyeon-Woo, Wonseok Choi, Nayeong Kim, Suha Kwak, and Tae-Hyun Oh. Exploiting synthetic data for data imbalance problems: baselines from a data perspective. *arXiv:2308.00994*, 2023. 1
- [86] Peter Young, Alice Lai, Micah Hodosh, and Julia Hockenmaier. From image descriptions to visual denotations: New similarity metrics for semantic inference over event descriptions. *TACL*, 2014. 10, 2
- [87] Zelin Zang, Hao Luo, Kai Wang, Panpan Zhang, Fan Wang, Stan Li, Yang You, et al. Boosting unsupervised contrastive learning using diffusion-based data augmentation from scratch. *arXiv:2309.07909*, 2023. 3, 8
- [88] Jure Zbontar, Li Jing, Ishan Misra, Yann LeCun, and Stéphane Deny. Barlow twins: Self-supervised learning via redundancy reduction. In *ICML*, 2021. 3, 7
- [89] David Junhao Zhang, Mutian Xu, Chuhui Xue, Wenqing Zhang, Xiaoguang Han, Song Bai, and Mike Zheng Shou. Free-atm: Exploring unsupervised learning on diffusion-generated images with free attention masks. *arXiv:2308.06739*, 2023. 3, 7
- [90] Tong Zhang, Congpei Qiu, Wei Ke, Sabine Süsstrunk, and Mathieu Salzmann. Leverage your local and global representations: A new self-supervised learning strategy. In *CVPR*, 2022. 3
- [91] Yifan Zhang, Daquan Zhou, Bryan Hooi, Kai Wang, and Jiasi Feng. Expanding small-scale datasets with guided imagination. In *NeurIPS*, 2023. 1

Multi-Source Adaptive Generative Augmentation for Quality-Driven Contrastive Representation Learning

Supplementary Material

1. Implementation Details of Methodology

1.1. Mechanisms for Controllable Synthesis

We generate synthetic views using a pretrained diffusion model $\mathcal{G}(\cdot)$ over T denoising steps, starting from a random Gaussian latent vector $\mathbf{z}_i \sim \mathcal{N}(0, \mathbf{I})$. To balance fidelity and diversity, we modulate two key hyperparameters:

Noise Level (ℓ): This parameter controls the intensity of visual perturbation applied to the image embedding in image-conditioned modes. We use [Stable unCLIP 2-1](#) as \mathcal{G} and extract the clean image embedding $\mathbf{c}_i^{\text{img}} = \mathcal{V}(\mathbf{I}_i)$ via its encoder \mathcal{V} . The perturbed embedding $\hat{\mathbf{c}}_i^{\text{img}}$ is obtained by injecting Gaussian noise ε :

$$\hat{\mathbf{c}}_i^{\text{img}} = \text{noisy}(\mathbf{c}_i^{\text{img}}, \ell) = \sqrt{\bar{\alpha}_\ell} \mathbf{c}_i^{\text{img}} + \sqrt{1 - \bar{\alpha}_\ell} \varepsilon,$$

where $\varepsilon \sim \mathcal{N}(0, \mathbf{I})$ and $\bar{\alpha}_\ell = \prod_{j=1}^{\ell} \alpha_j$ denotes the cumulative product of noise schedule variances following the standard DDPM [34] schedule. The model then generates a new view conditioned on $\hat{\mathbf{c}}_i^{\text{img}}$.

Guidance Scale (g): This parameter modulates textual alignment strength via Classifier-Free Guidance [33] in text-conditioned modes. Given a caption \mathbf{T}_i , we obtain the text embedding $\mathbf{c}_i^{\text{ext}} = \mathcal{T}(\mathbf{T}_i)$ via encoder \mathcal{T} . During each reverse step t , the noise estimate ϵ_t is computed by interpolating between the conditional and unconditional predictions (using a null caption \emptyset):

$$\epsilon_t = \mathcal{G}(\mathbf{z}_i, t, \emptyset) + g \cdot (\mathcal{G}(\mathbf{z}_i, t, \mathbf{c}_i^{\text{ext}}) - \mathcal{G}(\mathbf{z}_i, t, \emptyset)).$$

The scale g determines the relative weight of the text condition $\mathbf{c}_i^{\text{ext}}$ against the unconditional baseline. For view synthesis, we employ [Stable Diffusion v2-1-unCLIP](#) in the image-conditioned and image-text-conditioned modes, and [Stable Diffusion v2-1](#) in the text-conditioned mode.

1.2. Foreground Proportion Estimation

To estimate the foreground proportion in Step 1 of Sec. 4.2.1, we adopt the pretrained [CLIP ViT-H/14](#) backbone, which also serves as the conditional image encoder \mathcal{V} in [Stable UnCLIP v2-1](#). Given a 224×224 input, this backbone produces 256 tokens of dimension 1280. For PCA-based feature extraction, we randomly sample 10,000 images from the training set. The threshold α in Eq. 5 is chosen such that foreground tokens constitute roughly 40% of the total, ensuring a clear separation between foreground and background, as illustrated in Fig. 2.

1.3. Adaptive View Generation Details

For [IN1K](#), [CF10](#), [CF100](#), and [TinyIN](#), we generate one additional view per training image using the image-conditioned adaptive view generation method. The number of denoising steps T is set to 20 for computational efficiency, and the classifier-free guidance scale [33] is fixed to 10 to preserve image fidelity. The diversity of synthesized views is modulated by applying different noise perturbations to the image embeddings. To align with the input resolution of each dataset, the generated images are down-sampled from their native 768^2 resolution to 512^2 (IN1K), 32^2 (CF10 and CF100), and 64^2 (TinyIN).

For the Conceptual Captions 3M (CC3M) dataset [65], we adopt a hybrid data strategy: a portion of the data is enhanced with our multi-source adaptive view generation. Each enhanced image-text pair is expanded into a positive set (Eq. 3) using the three adaptive generation modes introduced in Secs. 4.2.1, 4.2.2, and 4.2.3. All images in these positive sets, including both original and generated views, are further processed by a standard augmentation pipeline. In the *comparison with multimodal methods* setting (Sec. 5.2), we train on the full CC3M dataset ($\sim 3\text{M}$ image-text pairs), where a 1M subset is enhanced by the adaptive generation strategy. For the *ablations on multimodal components* (Sec. 6.2), we train on a 1M subset of CC3M, within which only a portion (e.g., 100k or 500k samples) is enhanced, while the rest remain unmodified.

2. Experimental Details

2.1. Details for Vision Pretraining Comparisons

Pretraining Setup. We conduct experiments using both Convolutional (ResNet-18, ResNet-50 [28]) and Transformer (ViT-S, ViT-B [18]) backbones. ResNet-50 is the default architecture unless otherwise specified, while MoCov3 experiments also utilize ViTs. All models are pretrained on the ImageNet-1K (IN1K) dataset [15]. We strictly adhere to the original training configurations of each baseline method to ensuring fair comparison. Our adaptive generative augmentation is applied to the entire IN1K training set. Table 12 provides a detailed summary of the hyperparameters used for each framework (MoCov2, SwAV, SimSiam, BYOL, MoCov3). We reproduce MoCov3 baselines using the official implementation.

Linear Classification Protocol. After pretraining, we train a linear classifier on top of the frozen encoder using

Table 11. Pretraining hyperparameters used for comparison with vision representation learning methods on IN1K.

	MoCov2	SwAV	SimSiam	BYOL	MoCov3	MoCov3
Optimizer	SGD	LARS	SGD	LARS	LARS	AdamW
Learning Rate	0.03	0.6	0.05	4.8	1.2/9.6/4.8	2.4e-3
Weight Decay	1e-4	1e-4	1e-4	1e-6	1e-6	0.1
Momentum	0.9	0.9	0.9	0.9	0.9	-
Cosine Decay	✓	✓	✓	✓	✓	✓
Batch Size	256	256	256	4096	512/4096/4096	4096/4096
Loss	$\mathcal{L}_{img-img}^{sim}$	$\mathcal{L}_{img-img}^{kl}$	$\mathcal{L}_{img-img}^{cos}$	$\mathcal{L}_{img-img}^{cos}$	$\mathcal{L}_{img-img}^{sim}$	$\mathcal{L}_{img-img}^{sim}$
Epochs	200	200	200	200	100/300	300
Backbone	ResNet50	ResNet50	ResNet50	ResNet50	ResNet50	ViT-S/ViT-B
Embedding Dim	2048	2048	2048	2048	2048	384/768
Projection Dim	128	128	2048	256	256	256

IN1K. To ensure fairness, we adopt identical training hyperparameters across all baselines: 90 epochs, a batch size of 1,024, and the SGD optimizer with momentum 0.9 and no weight decay. A cosine learning rate schedule [49] is applied, with an initial learning rate of 0.4 for ResNet-based models and 12.0 for ViT-based models.

Transfer Learning on MS-COCO. To assess generalization to pixel-level tasks, we transfer the pretrained models to MS-COCO [48] for object detection and instance segmentation using the Mask R-CNN [29] framework with ResNet-50-FPN. Models are pretrained on IN1K for 200 epochs and fine-tuned on COCO train2017, evaluated on val2017 using the Detectron2 $1 \times$ schedule [79] (90k iterations, with learning rate decay at 60k and 80k).

2.2. Details for Vision-Language Comparisons

Pretraining Setup. Pretraining is conducted on the CC3M dataset [65], with 1M data enhanced by our multi-source adaptive view generation mechanism. We primarily adopt the ViT-B/16 backbone, and all reported results are based on ViT-B/16 unless otherwise noted (TripletCLIP uses ViT-B/32). Unless specified, vision-language models are pretrained for 40 epochs on 8 GPUs with a batch size of 64 per GPU. The AdamW optimizer is used with $\beta_1 = 0.9$, $\beta_2 = 0.98$, a base learning rate of 2×10^{-4} , weight decay of 0.1, and a 5-epoch warmup schedule.

Evaluation Benchmarks. The evaluation is performed on zero-shot image-text retrieval (MS COCO [48], Flickr30k [86], and Flickr8k [35]) and zero-shot/linear classification across ten diverse image classification datasets: ImageNet [15], CIFAR-10 [42], CIFAR-100 [42], Aircraft [50], DTD [14], Flowers [52], Pets [55], SUN397 [81], Caltech-101 [22] and Food-101 [5].

Linear Classification Protocol. For downstream image classification, we pretrain the vision encoder on CC3M, freeze its weights, and train a linear classifier on top. The classifier is trained for 90 epochs using SGD with a momentum of 0.9. Following standard practice, the base learning rate is selected from a sweep over $\{0.001, 0.002, 0.005, 0.01, 0.02, 0.05, 0.1, 0.2, 0.3, 0.5\}$. Additional hyperparameters for the ten classification

Table 12. Hyperparameters for linear classification.

	IN1K	CF10	CF100	Aircraft	DTD	Flowers	Pets	SUN397	Caltech-101	Food-101
GPUs	8	2	2	1	1	1	1	1	1	2
Batch/GPU	256	256	256	128	64	64	128	256	128	256
Drop last	True	True	True	False	False	False	False	True	False	True
Classes	1000	10	100	1000	47	102	37	397	101	101

datasets used in the linear probe are summarized in Tab. 12.

2.3. Details for GenView++(V) Component Ablations

We detail the experimental setup for the vision-only ablation studies presented in Sec. 6.1 of the main text.

Pretraining Setup. We use ImageNet-100 (IN100) [70], a class-balanced subset of ImageNet-1K, as the pretraining dataset. The backbone is a ResNet-18 trained using the MoCo v3 framework. We train for 100 epochs with a batch size of 512. We employ the LARS optimizer with a base learning rate of 1.2, weight decay of 1×10^{-6} , and momentum of 0.9. The learning rate follows a cosine decay schedule. To construct the pool of synthetic positive views, we randomly sample 50,000 images from IN100 (maintaining class balance) to serve as condition inputs for our Image-Conditioned generation module.

Evaluation Setup. We perform linear probing on the frozen encoder using the full IN100 dataset. The linear classifier is trained for 50 epochs. All other optimization settings (optimizer, augmentations) are consistent with the main ImageNet-1K linear evaluation protocol described in Appendix 2.1.

2.4. Details for GenView++(VL) Component Ablations

We detail the setup for the vision-language ablation studies presented in Sec. 6.2.

Pretraining Setup. All models utilize a ViT-B/16 backbone initialized with CLIP weights. Training is conducted on a 1M subset of CC3M. To evaluate the impact of our generation module, we replace a portion of the Models are trained for 25 epochs with a 2-epoch linear warmup. We use the AdamW optimizer with a peak learning rate of 4×10^{-4} (base learning rate 2×10^{-4}), weight decay of 0.1, and β coefficients $(\beta_1, \beta_2) = (0.9, 0.98)$. The training runs on 4 GPUs with a batch size of 64 per GPU.

Evaluation Setup. We evaluate the learned representations via linear probing on CIFAR-10 and ImageNet-100. A linear classifier is trained on top of the frozen backbone for 90 epochs using SGD (momentum 0.9, no weight decay) with a batch size of 256. Following StableRep [72], we determine the optimal base learning rate for each dataset by sweeping over the range 0.001, 0.002, 0.005, 0.01, 0.02, 0.05, 0.1, 0.2, 0.3, 0.5.

Table 13. Rule-based scoring instruction prompt R for evaluating visual complexity of caption inputs.

<pre>{ "role": "system", "content": "You are tasked with evaluating the visual complexity of a text prompt intended for image generation. Your goal is to assign a score from 1 to 4 that reflects how richly the prompt describes concrete visual elements. The more detailed and diverse the visual information, the higher the score should be. Visual complexity is determined by identifying constraints that directly affect how an image would be generated. These include the specificity of objects mentioned (such as type, quantity, or material), descriptive visual features (such as color, texture, or lighting), spatial relationships (such as layout or perspective), dynamic elements (such as actions or interactions), and stylistic cues (such as artistic genres or cultural elements). A prompt that contains a wide range of such features is considered more complex than one that simply names general categories. A prompt that only refers to broad object types without any additional visual information should be scored as 1. If it includes a small number of visual constraints—typically one to three—it should be scored as 2. A score of 3 is appropriate when the prompt contains a moderate level of detail, roughly four to six constraints. A prompt that includes more than six distinct and specific visual elements—such as combinations of materials, textures, color, spatial arrangement, and style—should be scored as 4. When evaluating, do not include abstract or emotional language that does not translate directly into visual features. Focus only on concrete and visualizable information. After analyzing the prompt, return a score from 1 to 4. Return the result in the following format: [score: ?]."} }</pre>
<pre>{ "role": "user", "content": f"Now output the score of visual constraints for the following text prompt: { }."}</pre>

3. Additional Experimental Results

3.1. Evaluation of Visual Complexity Estimation Precision

To validate the reliability of our adaptive guidance strategy (g_i^{ada}), we assess the precision of the automated complexity estimator (DeepSeek-2-Chat-Lite). We constructed a reference benchmark using 500 randomly sampled captions from the training set, with ground-truth complexity scores generated by GPT-4o and verified by human annotators. Our automated scorer was then evaluated against this ground truth using the rubric in Tab. 13. Results show 93.8% accuracy (within a ± 1 tolerance), confirming that our LLM-based scorer closely aligns with human percep-

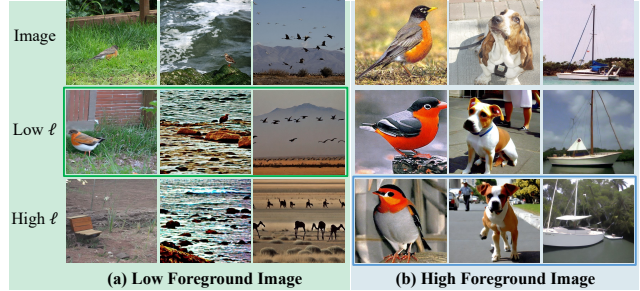


Figure 4. **Image-Conditioned Adaptive Generation.** The noise level ℓ is adapted to the image’s foreground proportion. (a) For low-foreground images, a low ℓ (green boxes) avoids semantic drift, object loss, or distortion (Col 1–3). (b) For high-foreground images, a high ℓ (blue boxes) enriches diversity, e.g., varying pose (Col 4), action (Col 5), and background (Col 6).

tion and enables complexity-aware generation control.

3.2. Visualization of Adaptive Generation

Figures 4, 5, and 6 provide qualitative validation of our adaptive strategies, demonstrating how dynamic parameter modulation prevents common generative failure modes.

Image-Conditioned (Fig. 4): We observe that small or indistinct subjects (Panel a) are highly sensitive to noise; a high ℓ (row 3) often causes the object to vanish or distort. Our strategy correctly assigns a low ℓ (green boxes) to preserve semantic fidelity. Conversely, salient subjects (Panel b) remain robust under high noise, allowing us to safely introduce significant background and pose variations.

Text-Conditioned (Fig. 5): Detailed captions (Panel a) already constrain the generation space; adding high guidance results in rigid, repetitive outputs. Our method relaxes guidance (g) to foster diversity. For simple captions (Panel b), high guidance is essential to prevent semantic drift, ensuring the generated image remains faithful to the limited textual cues.

Image-Text-Conditioned (Fig. 6): This visualizes the synergy of both strategies. The grid demonstrates that our method consistently selects the optimal parameter combination (green/highlighted boxes). For instance, for semantically rich captions (Panel a & b), a lower guidance scale encourages diverse generation, while simpler captions (Panel c & d) benefit from a higher guidance scale to maintain semantic alignment. Meanwhile, low-saliency images (a & c) require a lower noise level to preserve fine details, whereas high-saliency images (b & d) tolerate a higher noise level to enable greater visual variation.

3.3. Computational Cost and Efficiency

In this section, we analyze the trade-off between the one-time generation cost and the long-term benefits in training efficiency and model performance.



Figure 5. **Text-Conditioned Adaptive Generation.** The guidance scale g is adjusted by caption complexity. (a) Detailed captions with high visual complexity: a low g (green boxes) encourages diverse generations while preserving fine semantics. In contrast, a high g over-constrains the output, yielding repetitive or rigid results. (b) Simple captions with low visual complexity: a high g (blue boxes) strengthens text-image alignment and ensures key concepts are retained.

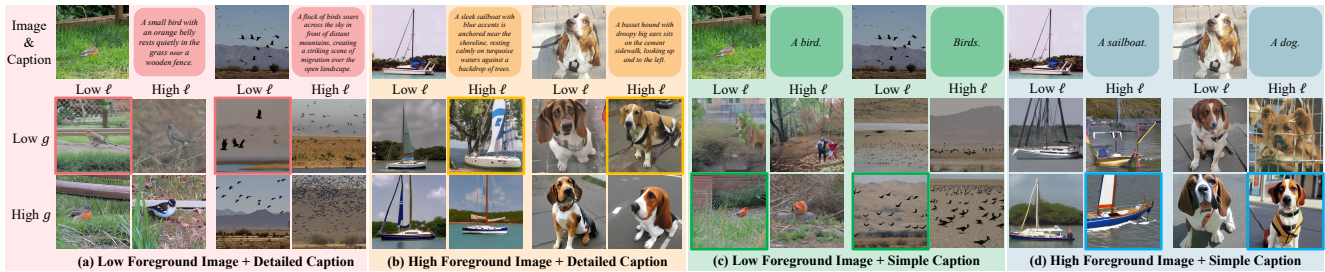


Figure 6. **Image-Text-Conditioned Adaptive Generation.** This mode jointly adapts noise level ℓ and guidance scale g for fine-grained cross-modal control. (a) Low-foreground + detailed captions: low ℓ preserves small subjects and low g promotes diverse poses and environments (pink boxes); high ℓ or g leads to semantically mismatches (e.g., Row 2, Col 2) or reduced diversity (e.g., Row 3, Col 1). (b) High-foreground + detailed captions: high ℓ enriches variation and low g avoids over-constraining by text (yellow boxes); low ℓ or high g limits diversity. (c) Low-foreground + simple captions: low ℓ preserves subjects while high g enforces text grounding (green boxes); low g induces weak textual constraints, risking semantic drift from the intended concept (e.g., unrelated humans in Row 2, Col 10). (d) High-foreground + simple captions: jointly high ℓ and g produce diverse yet consistent generations grounded in strong visual anchors and minimal text.

One-Time Offline Investment vs. Recurring Training Cost. It is crucial to distinguish between *setup cost* and *training cost*. While generating synthetic views requires GPU hours, this is a one-time, offline investment. Unlike online augmentations that consume CPU/GPU resources during every training iteration, our adaptive generation is performed once to construct a static pool of positive views. This generated dataset can be:

- **Reused indefinitely** across different model architectures (e.g., ResNet, ViT), varying hyperparameters, and diverse downstream tasks without re-generation.
- **Shared with the community**, effectively amortizing the initial generation cost to zero for future researchers.

From a lifecycle perspective, the initial generation cost becomes negligible when amortized over multiple training runs and architectural explorations.

Superior Data Efficiency. The core value of GenView++ lies in replacing "quantity" with "quality". As demonstrated in Table 3, GenView++ achieves higher accuracy (**65.62%**) using only 0.15M generated views compared to expand-

ing the dataset with 0.3M real images from ImageNet-21K (64.10%). This implies that our adaptive views carry higher information density than random real-world samples. Consequently, GenView++ enables models to learn robust representations with fewer training samples, potentially reducing the total training epochs required to reach target performance compared to pretraining on massive, noisy web-crawled datasets (e.g., LAION-400M).

Scalability. Since the generation process is fully parallelizable and does not require gradients or backpropagation, it can be efficiently scaled on CPU clusters or inference-optimized GPUs, further lowering the barrier to adoption.